

Atmospheric mesoscale conditions during the Boothbay meteotsunami: a numerical sensitivity study using a high-resolution mesoscale model

Kristian Horvath · Ivica Vilibić

Received: 1 July 2013 / Accepted: 11 January 2014 / Published online: 4 February 2014
© Springer Science+Business Media Dordrecht 2014

Abstract The article aims to test the sensitivity of high-resolution mesoscale atmospheric model to fairly reproduce atmospheric processes that were present during the Boothbay Harbor meteotsunami on 28 October 2008. The simulations were performed by the Weather and Research Forecasting (WRF) model at 1-km horizontal grid spacing by varying initial conditions (ICs) and lateral boundary conditions (LBCs), nesting strategy, simulation lead time and microphysics and convective parameterizations. It seems that the simulations that used higher-resolution IC and LBC were more successful in reproduction of precipitation zone and surface pressure oscillations caused by internal gravity waves observed during the event. The results were very sensitive to the simulation lead time and to the choice of convective parameterization, while the choice of microphysics parameterization and the type of nesting strategy (one-way or two-way) was less important for reproducibility of the event. The success of the WRF model appears limited to very short-range forecasting, most advanced parameterizations, and very high-resolution grid spacing; therefore, the applicability of present atmospheric mesoscale models to future operational meteotsunami warning systems still has a lot of room for improvements.

Keywords Mesoscale atmospheric model · Sensitivity study · Boothbay meteotsunami

1 Introduction

Meteotsunamis or meteorological tsunamis are destructive ocean waves in a tsunami frequency band that are found to occur in coastal areas of the World Ocean satisfying several

K. Horvath (✉)
Meteorological and Hydrological Service, Grič 3, 10000 Zagreb, Croatia
e-mail: kristian.horvath@cirus.dhz.hr

I. Vilibić
Institute of Oceanography and Fisheries, Šetalište I. Meštrovića 63, 21000 Split, Croatia

conditions on surrounding bathymetry and meteotsunami source (listed by Monserrat et al. 2006). While the propagation and coastal inundation is following the “ordinary” tsunami physics, generation of a meteotsunami is a multi-resonant phenomenon having origin in the atmosphere. A travelling air-pressure disturbance, normally associated with storms, gravity waves of short wavelengths (typically from 10 to 50 km), squall lines, pressure jumps and similar, may excite long ocean waves if the speed of the disturbance is equal to the speed of long ocean waves (Proudman 1929), which is dependable on the ocean depth only. The atmospheric forcing and resonant conditions should encompass a wider coastal area covering several wavelengths of the disturbance in order to generate a significant meteotsunami wave (Vilibić 2008). The generated wave travelling towards the coastline is then amplified by the topography and finally multiplied in a harbour or bay through harbour resonance, which is efficient for funnel-shaped and elongated coastal basins with large top-to-mouth amplification factors (Rabinovich 2009).

While the ocean dynamics of meteotsunami waves is not too complicated and is mostly dependant of the topography of a region, the source in the atmosphere has not been easy to investigate due to high temporal and spatial changes of small-scale processes normally associated to the event. A network of microbarographs was the first observational network that was used for capturing of the atmospheric disturbance responsible for meteotsunami generation and for supporting theoretical investigations (Orlić 1980; Hibiya and Kajiuura 1982; Monserrat et al. 1991). In addition, the analyses of synoptic charts and contemporary atmospheric conditions were performed during meteotsunami events, pointing out to common synoptic conditions found during meteotsunamis (Jansà et al. 2007; Šepić et al. 2012). However, a full reproduction of the meteotsunami source processes in the atmosphere was achieved just recently, when the mesoscale atmospheric models become capable to fairly reproduce the physics at the mesoscale (Belušić et al. 2007; Šepić et al. 2009; Tanaka 2010; Renault et al. 2011).

Up to date, only the study by Renault et al. (2011) used coupled atmosphere–ocean modelling system and fairly reproduced the whole process, from the source in atmosphere to the meteotsunami dynamics in the ocean, which might be eventually used in the operative forecasting of a meteotsunami event. Presently, the only operational meteotsunami system, placed on the Balearic Islands, is based on analysis of synoptic conditions and provides qualitative forecast of the meteotsunami danger a few days in advance (Jansà et al. 2007). However, the difference and quantitative mismatching of modelling system results versus observations allow for improvements, both in atmosphere and ocean parts of the system. Hence, our study is concentrated to the reproduction of atmospheric source of a recent meteotsunami event, that is preformed through sensitivity studies and variation in different simulation parameters and schemes that are present in the state-of-the-art numerical weather forecast models.

The examined event occurred in Boothbay Harbor and surrounding area on 28 October 2008, with eyewitnessed rapid sea-level variations ranging up to 4 m. By examining all available atmospheric and oceanographic data and by applying Weather and Research Forecasting (WRF) model, Vilibić et al. (2014) described the meteotsunami source in the atmosphere and found that onshore travelling internal gravity waves (IGWs), ducted with weak dissipation in lower troposphere and capped by an instability, occurred simultaneously with meteotsunami ocean waves. Therefore, ground air-pressure oscillations connected with IGWs were presumably responsible for the resonant forcing and generation of long ocean waves in the shelf area. This study will go a step forward: it will investigate the applicability of the WRF model to a proper reproduction of the atmospheric conditions during a meteotsunami, by varying initial and lateral boundary conditions, nesting strategy,

simulation lead time and microphysics and convective parameterizations. Finally, a discussion about the applicability of the results in an operational meteotsunami forecasting model will be provided.

2 Data and methods

The mesoscale model used in this study is the mass-core Advanced Research version of the Weather Research and Forecasting model (WRF) (Skamarock and Klemp 2008). WRF is a non-hydrostatic primitive equation model that has the terrain-following pressure as the vertical coordinate (Laprise 1992). For temporal discretization, time splitting is used to maintain the numerical stability; the low-frequency modes are integrated using the third-order accuracy integration scheme. Numerical discretization is performed on Arakawa C-grid with a fifth-order horizontal advection scheme.

The control mesoscale model set-up consists of three nested domains (Fig. 1), with the horizontal grid spacing of 9, 3 and 1 km, respectively, and 40 vertical levels. The set of parameterizations used in the control WRF model set-up included Morrison two-moment microphysics parameterization, Grell–Devenyi cumulus parameterization (only outermost domain), and Mellor–Yamada–Janjić planetary boundary layer turbulence parameterization (Mellor and Yamada 1974, 1982; Janjić 2001). Dudhia scheme was used for parameterization of short-wave radiation (Dudhia 1989), and the rapid radiative transfer model was chosen to parameterize long-wave radiation (Mlawer et al. 1997). The Noah land-surface model (Chen and Dudhia 2001; Ek et al. 2003) was used to simulate the vertical transport of soil moisture and heat. The model was set up not to damp vertical velocities and with reduced amount of explicit smoothing. Computational time step was 6 s in the innermost domain.

The exact conditions leading to meteotsunamis are often hard to simulate with current state-of-art mesoscale models, including the WRF model. Therefore, the numerical experiments were designed to address the sensitivity of model results to:

1. Initial and boundary conditions (ICs and LBCs), since the atmospheric conditions generating meteotsunamis are challenging to model and predict, and small uncertainties in ICs and LBCs may have a large influence on mesoscale simulation results.
2. Convective parameterization, since meteotsunamis may occur associated with convective activity (Belušić and Strelec-Mahovic 2009), such as observed during the Boothbay event. In addition, some of the mechanisms proposed for generating atmospheric conditions favouring meteotsunamis are wave-CISK (Belušić et al. 2007), the interaction between deep convection and internal gravity waves (IGWs).
3. Microphysics parameterization, since it controls the explicit precipitation (both convective and stratiform) in higher-resolution modelling domains when convective parameterization is switched off.
4. Nesting strategy that may be classified as one-way or two-way. In the one-way nested simulations, results from higher-resolution domains do not influence results of the lower-resolution domains. In two-way nesting set-up, the results from the higher-resolution domains propagate to lower-resolution domains. Thus, two-way interaction may be important for flow evolution in general, and especially for some of the proposed meteotsunami mechanisms, such as the trapping of IGWs or their interaction with the convection (wave-CISK). On the other hand, in two-way nesting set-up with a typical grid nesting ratios of 3 or 4 IGWs of wavelengths smaller than 10 dx in certain

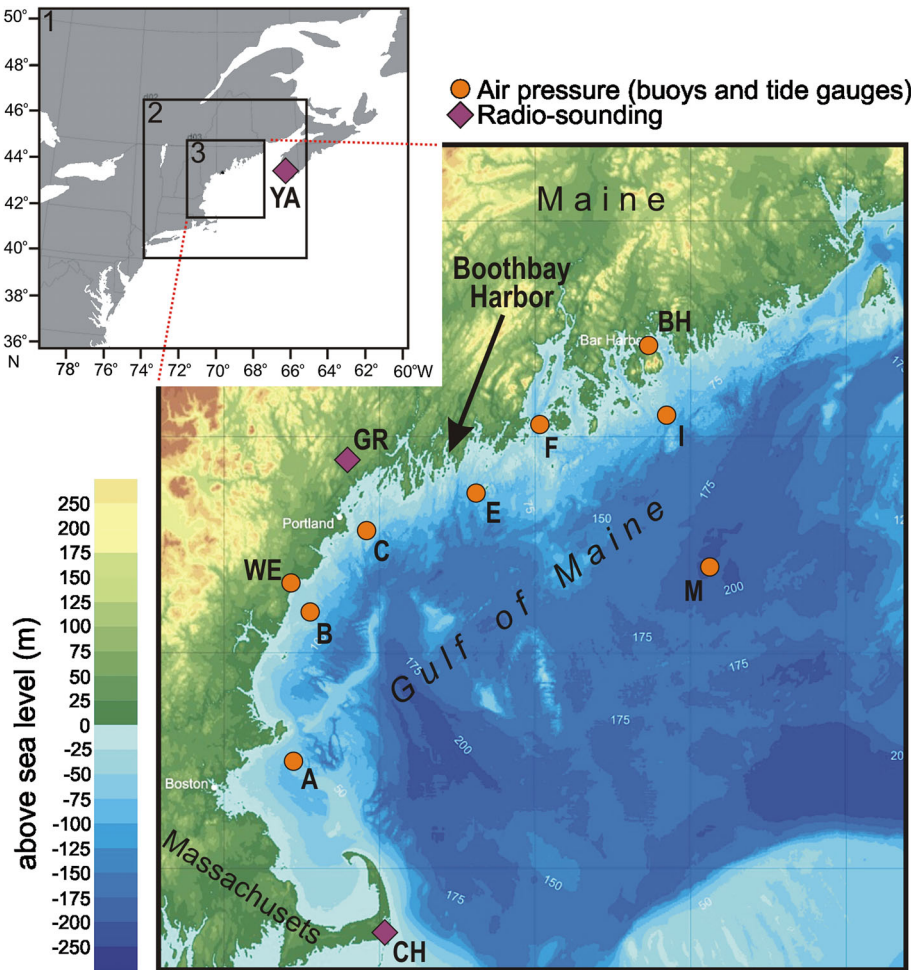


Fig. 1 Investigated area with positions of tide gauges and buoys where air pressure has been measured (circles) and sounding stations (diamonds). The position of Boothbay Harbor is indicated by an arrow. The domains used for the WRF modelling are labelled by 1, 2 and 3

conditions may be numerically aliased in the lower-resolution domain (Schroeder and Schlünzen 2009). Though two-way nesting should in principle lead to more accurate results, most implementations of the operational numerical weather prediction models use one-way nesting. Therefore, the analysis of results using the type of nesting is important also for assessment of potentials for numerical prediction of atmospheric conditions related to meteotsunamis.

5. Simulation lead time, for investigating potentials of relying on mesoscale models in early warning systems related to meteotsunamis. The computational cost of the numerical experiment with 24-h simulation lead time reached one thousand processor hours.

The verification of the model simulations is performed on available radio-sounding data, reanalysis fields, radar and satellite imagery (position of ground stations may be

found in Fig. 1). Radio-sounding stations Chatman (CH), Gray (GR) and Yarmouth (YA) are obtained from University of Wyoming Web site (<http://weather.uwyo.edu/upperair/sounding.html>). Geostationary Operational Environmental Satellite (GOES)—12 infrared window channel (10.7 μm) brightness temperature data were retrieved from NOAA CLASS system (http://www.class.ngdc.noaa.gov/saa/products/search?datatype_family=GVAR_IMG), while mosaic composite radar reflectivity data used for verification of the model results originated from NEXRAD WSR-88D Doppler radars.

In this article, we focus primarily on verification of horizontal and vertical spatial structure of the atmosphere, and we restrain from verifying model simulations with in situ buoy air-pressure data. This type of verification was performed for the control simulation (cf. Fig. 8 from Vilibic et al. 2014), but since (1) no buoy data were available on locations where large sea-surface oscillations were recorded, (2) both buoys and coastal stations had insufficient resolution (which should be 1 min or less) for proper representation of a meteotsunami, and (3) rapid large-amplitude MSLP oscillations were not recorded at any of the buoys in the area, evaluation tackled only larger-scale aspects of model simulation. As discussed in Vilibic et al. (2014), the frequency of the measured data was sufficient neither for an in-depth analysis of the high-frequency air-pressure oscillations associated with the Boothbay meteotsunami nor for a quantitative verification of the air-pressure variability in the WRF model results.

Finally, we recognize that other aspects of the simulations may be chosen for a meaningful more detailed analysis, such as vertical structure of IGWs and convective cells, generation and sustainability of the wave ducting layer and propagation speed of IGWs. Likewise, attempt to simulate sea-surface oscillations was not done in this study. While these are all valid approaches, we chose to focus as much as possible the joint forcing of all atmospheric processes on the intermediary between atmosphere and the ocean—as represented by mean sea-level pressure oscillations—and at the same time, verify horizontal and vertical structure of the atmosphere by the available remote sensing and radio-sounding measurements.

3 Results

3.1 Verification and sensitivity to initial and lateral boundary conditions

The control mesoscale model simulation was initialized at 12 UTC 28 October 2008 for a 12-h period. To assess the role and sensitivity to initial and lateral boundary conditions (IC and LBC), three sensitivity simulations were performed using different sources of global model (re)analysis data used for initial (IC) and lateral boundary conditions (LBC). In addition, the sensitivity analysis studied the effects of the type of interaction among domains—that is, one-way or two-way nesting. IC and LBC were provided by the following sources:

1. North-American regional reanalysis (NARR, grid spacing $\sim 0.333^\circ$)
2. ERA-Interim (T255, grid spacing $\sim 0.75^\circ$)
3. ECMWF operational analysis, ECMWF-OA (T799, grid spacing $\sim 0.22^\circ$).

The first two datasets are reanalysis data, which use a long cut-off window for data assimilation and thus more observational data in the process of data assimilation at the lower grid spacing, while the last one is the operational short cut-off analysis which uses less observational data at the higher grid spacing.

Synoptic setting was similar in all global model (re)analysis: at 12 UTC 28 Oct 2008, a deep cyclone with a defined thermal structure (warm and cold cyclone sectors) located southwest of the Boothbay area moved towards the northeast (Fig. 2). The subtle differences between these datasets, however, did exist; note the differences in position and shape of warm sector, fronts, location of the jet streak and its intensity, properties of the dry upper-level air surge and the depth of the cyclone centre. As we will see later, these differences were large enough to cause a substantially different mesoscale flow evolution. The complete list of experiments, aimed at assessing the sensitivity of mesoscale simulations to the source of ICs and LBCs, is listed in Table 1.

A comparison of model results from one-way nested intermediate WRF domain ($dx = 3$ km) and measured radio-sounding data at 00 UTC 29 October 2008 is shown in Fig. 3. Generally, all simulations performed satisfactorily, but overestimated the moisture content in the upper troposphere. Some other differences are, however, notable: at Gray, which is the closest radio-sounding to Boothbay, the moisture content of the lower and middle layers was underestimated in simulation driven by NARR data—in accordance with the aforementioned fact that in NARR reanalysis Boothbay was not in the warm sector of the cyclone. On the other hand, the simulation driven with NARR performed the best farther north at Yarmouth.

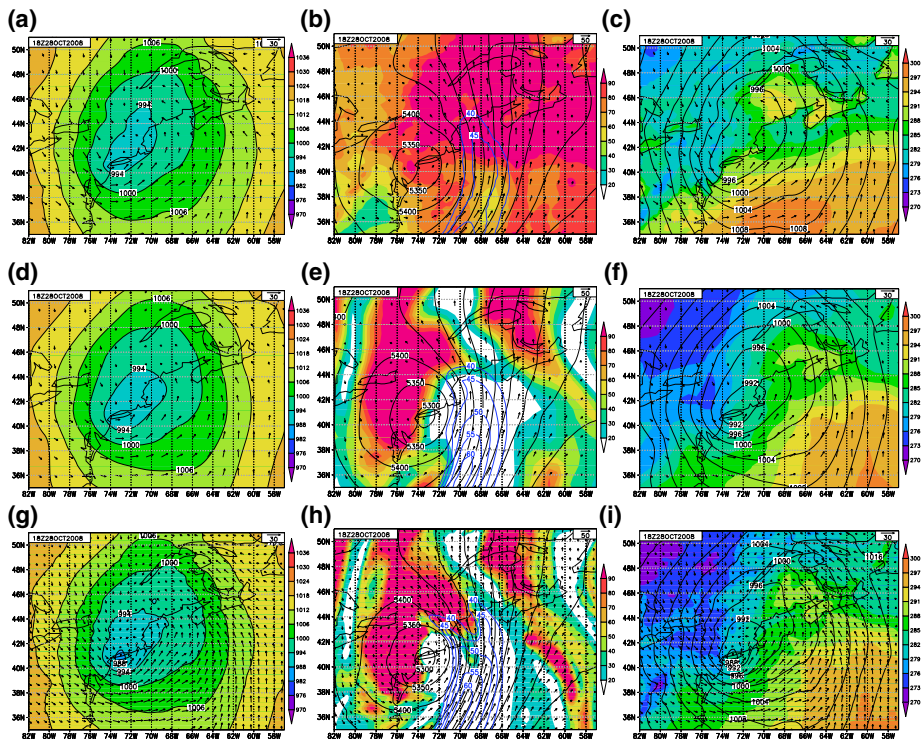


Fig. 2 Mean sea-level pressure (hPa, both shaded and in black contours, interval 6 hPa) and 10-m wind vectors for **a** NARR, **d** ERA-Interim and **g** ECMWF-OA, geopotential height (gpm, black contours), relative humidity (%), wind vectors and wind speed (ms^{-1} , purple contours starting at 40 ms^{-1} , interval 5 ms^{-1}) at 500 hPa for **b** NARR, **e** ERA-Interim and **h** ECMWF-OA, and T at 2 m AGL (K, shaded), mean sea-level pressure (hPa, contours, interval 3 hPa) and 10-m wind vectors for **c** NARR, **f** ERA-Interim and **i** ECMWF-OA at 18 UTC 28 October 2008

Table 1 List of experiments performed to assess the roles of initial and lateral boundary conditions

Exp. no.	1	2	3	4	5	6
IC and LBC	NARR	NARR	ERA-Interim	ERA-Interim	ECMWF-OA	ECMWF-OA
Nesting type	One-way	Two-way	One-way	Two-way	One-way	Two-way

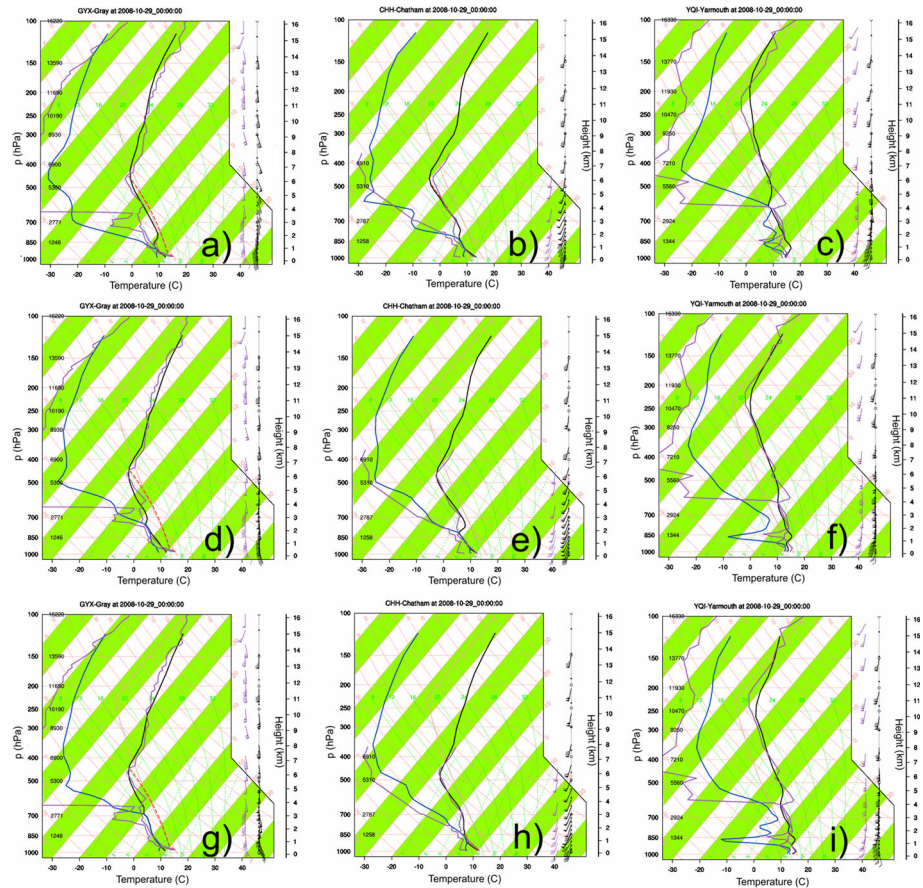


Fig. 3 Skew-T diagrams from one-way nested WRF domains 2 ($\Delta x = 3$ km) at Gray for **a** NARR, **d** ERA-Interim and **g** ECMWF-OA, Chatham for **b** NARR, **e** ERA-Interim and **h** ECMWF-OA and Yarmouth for **c** NARR, **f** ERA-Interim and **i** ECMWF-OA initial and lateral boundary conditions at 00 UTC 29 October 2008. Measured data are all in purple colour, and modelled data are in blue for dew point temperature and black for temperature and winds

Time series of measured and modelled buoy data (Fig. 8 in Vilibic et al. 2014) show that in all model experiments, the large-scale pressure tendency (decrease) was accurately simulated. Embedded in the large-scale pressure tendency, moderate pressure oscillations at buoy E were recorded between 17 UTC and 20 UTC 28 October 2008. This wave train of surface pressure oscillations was likely caused by internal gravity waves aloft (Vilibic et al. 2014). While WRF driven with NARR and ECMWF-OA in hours around and prior to

the Boothbay meteotsunami (18–19 UTC 28 October 2008) showed rapid pressure changes in the vicinity of buoy E, the simulation driven with ERA-Interim data showed a smooth decrease in pressure without rapid pressure changes on the scales relevant to meteotsunamis. Thus, we conclude that both simulations driven with ERA-Interim data are of limited use for our analysis.

Since a precipitation band moved over the Boothbay area around the time of meteotsunami, the analysis of the outgoing long-wave radiation was compared with the GOES IRW imagery (the imagery is shown in Fig. 6 by Vilibic et al. 2014). The comparison with model simulations (Fig. 4) suggest that WRF results driven with ERA-Interim and ECMWF-OA data were of reasonable accuracy in simulating the movement and shape of the cloud and precipitation band. In contrast, neither the shape nor the evolution of the cloud band was satisfactorily simulated in WRF simulation driven with NARR data. Therefore, simulation driven with NARR data did not succeed in reproducing the exact mesoscale details of the associated precipitation band.

Model simulated radar reflectivity at 19 UTC 28 October 2008 shows that simulations driven with ERA-Interim and ECMWF-OA were more accurate than the simulation driven with NARR data (Fig. 5, compare with Fig. 7 of Vilibic et al. 2014). Simulations driven by ERA-Interim and ECMWF-OA were generally similar; however, notable differences did exist. The reflectivity structures in simulations driven with ERA-Interim lacked intensity over the ocean south of the Boothbay area. In addition, the width of the squall line crossing Boothbay considerably narrowed towards the SE, in contrast to simulation driven with ECMWF-OA. In the latter, more convection was found over the ocean south of Boothbay, and the width of the precipitation system remained constant towards the SE, providing more similarity with observed radar imagery. On the other hand, excessive convective activity farther offshore south of Boothbay was simulated in experiment driven with ECMWF-OA. Neither of the simulations reproduced wave-like reflectivity bands oriented SW-NE near the southeast end of the precipitation system. However, mid-tropospheric internal gravity waves of similar scales in the Boothbay area were found in the model simulations driven with ECMWF-OA (Vilibic et al. 2014).

The mean sea-level pressure (MSLP) and wind vectors for simulations driven with the NARR, ERA-Interim and ECMWF-OA are shown in Fig. 6. At the approximate time of the Boothbay event (19 UTC 28 October 2008), elongated high-pressure band associated with the precipitation system moved over the Boothbay area. This high-pressure band moved northward in the WRF simulation driven by ECMWF-OA, but was not simulated in

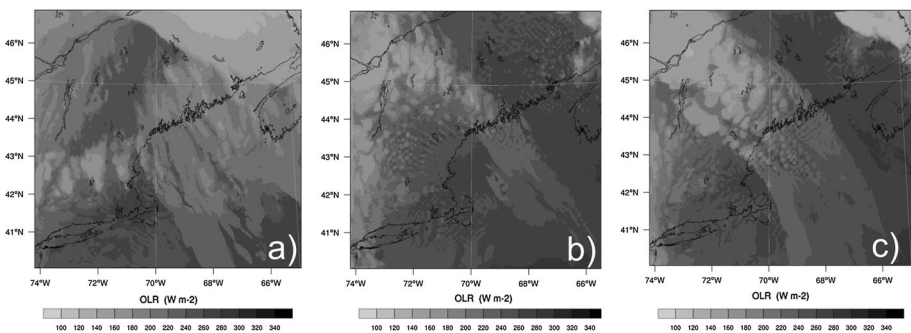


Fig. 4 Outgoing long-wave radiation (Wm^{-2}) at 19 UTC 28 October 2008 in one-way nested WRF simulations using **a** NARR, **b** ERA-Interim and **c** ECMWF_OA initial and lateral boundary conditions

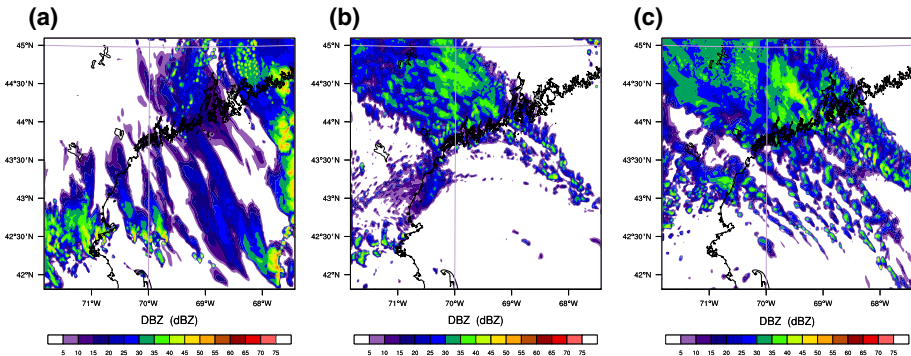


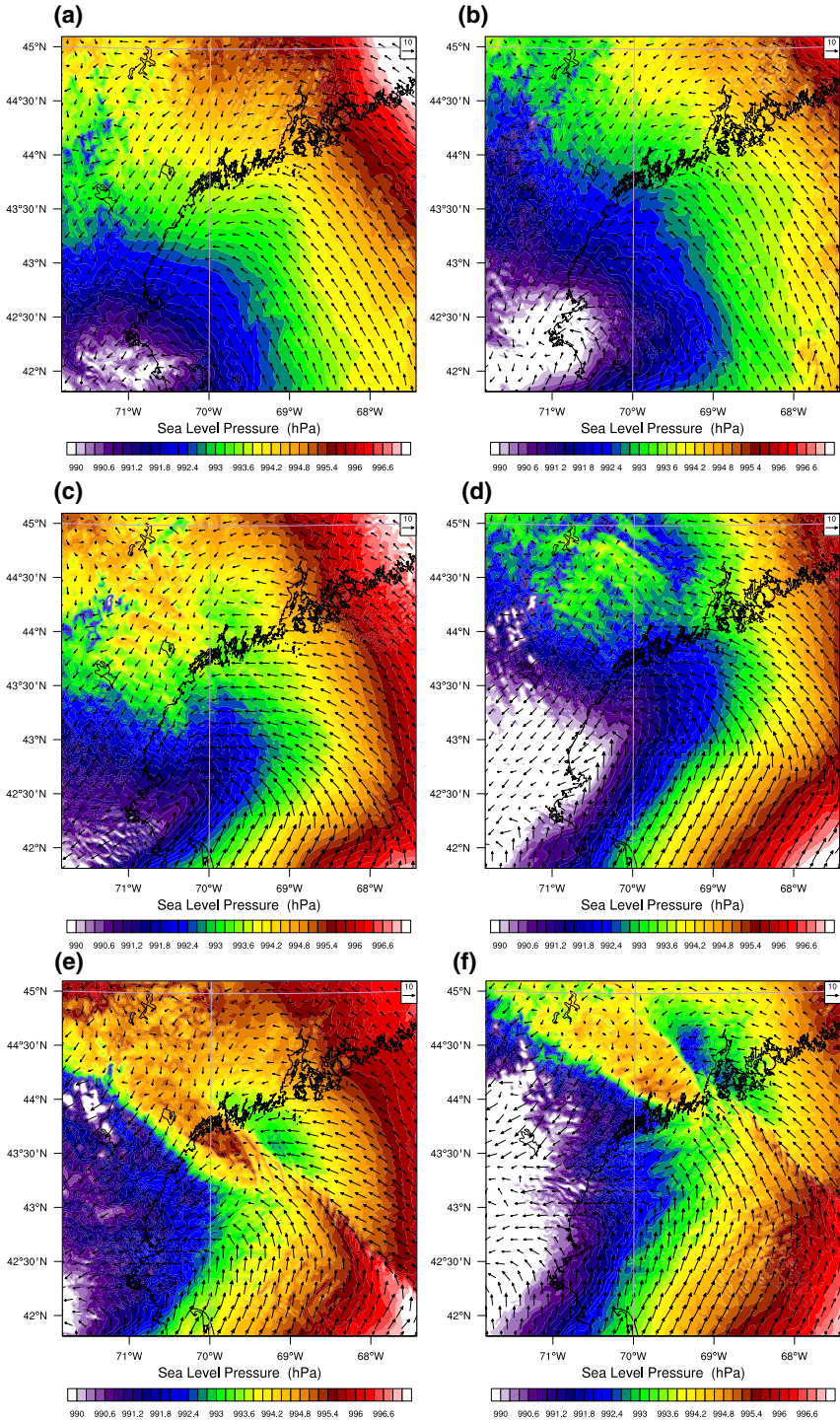
Fig. 5 Simulated radar reflectivity (DBZ) of the precipitation system moving over Boothbay at 19 UTC 28 October 2008 in one-way nested WRF simulations using **a** NARR, **b** ERA-Interim and **c** ECMWF-OA initial and lateral boundary conditions

experiments driven with either of the reanalysis. The timescale of the travelling high-pressure band was ~ 35 min, and its spatial scale was ~ 50 km. On the rear end of the high-pressure band, MSLP oscillations with lines of constant phase oriented W–E (WSW–ENE) propagated towards the coast. It may be noted even stronger isolated oscillatory pattern of MSLP was simulated some 100 km west of Boothbay in WRF simulation driven by ERA-Interim data. However, those pressure oscillations had lines of constant phase NW–SE, and the entire system moved from SSW to NNE. Concerning that both buoy and satellite analysis suggested that pressure disturbance that caused the Boothbay meteotsunami moved from SSE (SE) to NNW (NW) (Vilibic et al. 2014), we consider that the simulated MSLP field in numerical experiments driven with ERA-Interim is less appropriate for further analysis than are simulations driven with ECMWF-OA.

Thus, several aspects point to the fact that the best results were achieved in numerical simulations driven with ECMWF-OA. In experiments driven with NARR, simulated shape, position and intensity of the modelled cloud band as well as the low-level conditions (Gray sounding) were of inadequate accuracy. Experiments driven with ERA-Interim were quite successful, but did not show any pressure oscillations in the vicinity of Boothbay in the time window of ± 2 h around 19 UTC 28 October 2008. Results of these simulations also lacked convective activity over the ocean, which may be of interest for atmospheric triggering of meteotsunamis. While it is likely that differences between ECMWF-OA and ERA-Interim arise primarily due to differences in horizontal grid resolution, this may not necessarily be in case of NARR data that use different numerical weather prediction model and data assimilation procedure. Furthermore, we note that results were not very sensitive to the choice of the one-way or two-way nesting strategy as far as synoptic or gross mesoscale environment is concerned (not shown). However, it is expected that for numerical simulations of moist IGWs in the atmosphere such as observed by radar imagery southeast of Boothbay, the choice of nesting strategy may affect the modelling results, what will be further studied in the Sect. 3.5.

3.2 Sensitivity to the simulation lead time

To assess the sensitivity of model results to the simulation lead time, four additional numerical experiments were performed. Two simulations (one-way and two-way) were



◀ **Fig. 6** Simulated MSLP (hPa) and 10-m wind vectors in the one-way nested WRF simulations at 18 UTC 28 October 2008 using **a** NARR, **c** ERA-Interim and **e** ECMWF-OA initial and lateral boundary conditions and at 19 UTC 28 October 2008 using **b** NARR, **d** ERA-Interim and **f** ECMWF-OA initial and lateral boundary conditions. *White circles* are indicating ground stations used for model verification

initiated at 06 UTC 28 October 2008, and two simulations were initialized at 00 UTC 28 October 2008 using ECMWF-OA reanalysis for ICs and LBCs (Table 2).

Simulated radar reflectivity (Fig. 7) suggested that increasing the simulation lead time decreased the accuracy of modelling results. Indeed, notably different results regarding the properties of the precipitation band moving over Boothbay were found in the simulation initiated 6 h prior to the control simulation (initiated at 06 UTC 28 October 2008, which is approximately 15 h prior to the meteotsunami event) and the control simulation. As indicated by radar imagery, in simulation initiated at 06 UTC 28 October 2008, the precipitation zone was too weak and lacked a prominent squall line elongated NW–SE in the front of the precipitation zone. Similar was the case for simulations initiated at 00 UTC 28 October 2008 in which radar reflectivity resembled the results from simulation initiated at 12 UTC 28 October 2008 but nevertheless showed larger discrepancies when compared with radar imagery, such as too weak convective activity in the vicinity of the Boothbay area and offshore. Furthermore, mean sea-level pressure distribution in all four numerical experiments with longer simulation lead time showed no clues of the pressure oscillations relevant for the onset of the Boothbay meteotsunami.

3.3 Sensitivity to microphysics parameterizations

Microphysical parameterizations provide atmospheric heat and moisture tendencies and determine surface rainfall. Sensitivity to microphysics was performed by changing the default two-moment six-class Morrison parameterization to simpler one-moment five-class Lin (Purdue) parameterization (Table 3). Though more simple, Lin parameterization is a research parameterization often considered too computationally costly to be used in operational NWP. All simulations were performed with ECMWF-OA ICs and LBCs.

Comparison of one-way nested numerical experiments at 18:30 UTC 28 October 2008 suggested generally similar mesoscale evolution of the system in both simulations. Simulated mesoscale radar reflectivity in experiment with Lin parameterization was generally similar to the results obtained with the Morrison parameterization (Fig. 8). Lin parameterization did produce slightly stronger reflectivity especially in the southern part of the domain. However, comparison with radar data showed that in this area, even the control simulation with Morrison scheme provided excessive reflectivity (cf. Fig. 7 from Vilibic et al. 2014). Therefore, results of sensitivity simulation with the Lin parameterization appeared somewhat less accurate than results with the Morrison microphysics parameterization.

Simulated mesoscale surface pressure distribution was similar in both experiments. Nevertheless, simulated meso- γ scale structure of the pressure field in the vicinity of Boothbay was not alike due to different organization of individual troughs and ridges in the MSLP (Fig. 9). This is likely due to differences in simulated organization of the convection and/or IGWs aloft. The differences among simulations were moderate, and none of the experiments simulated pressure oscillations in the vicinity of the Boothbay area. In summary, the effects of microphysics parameterizations were not large enough to produce qualitatively different results, but the choice of microphysics schemes can still influence the representation of the individual pressure oscillations and cloud formations within the precipitation zone.

Table 2 List of experiments performed to assess the roles of the simulation lead times

Exp. no.	7	8	9	10	11	12
Initial time	00 UTC 28 Oct 2008	00 UTC 28 Oct 2008	06 UTC 28 Oct 2008	06 UTC 28 Oct 2008	12 UTC 28 Oct 2008	12 UTC 28 Oct 2008
Nesting type	One-way	Two-way	One-way	Two-way	One-way	Two-way

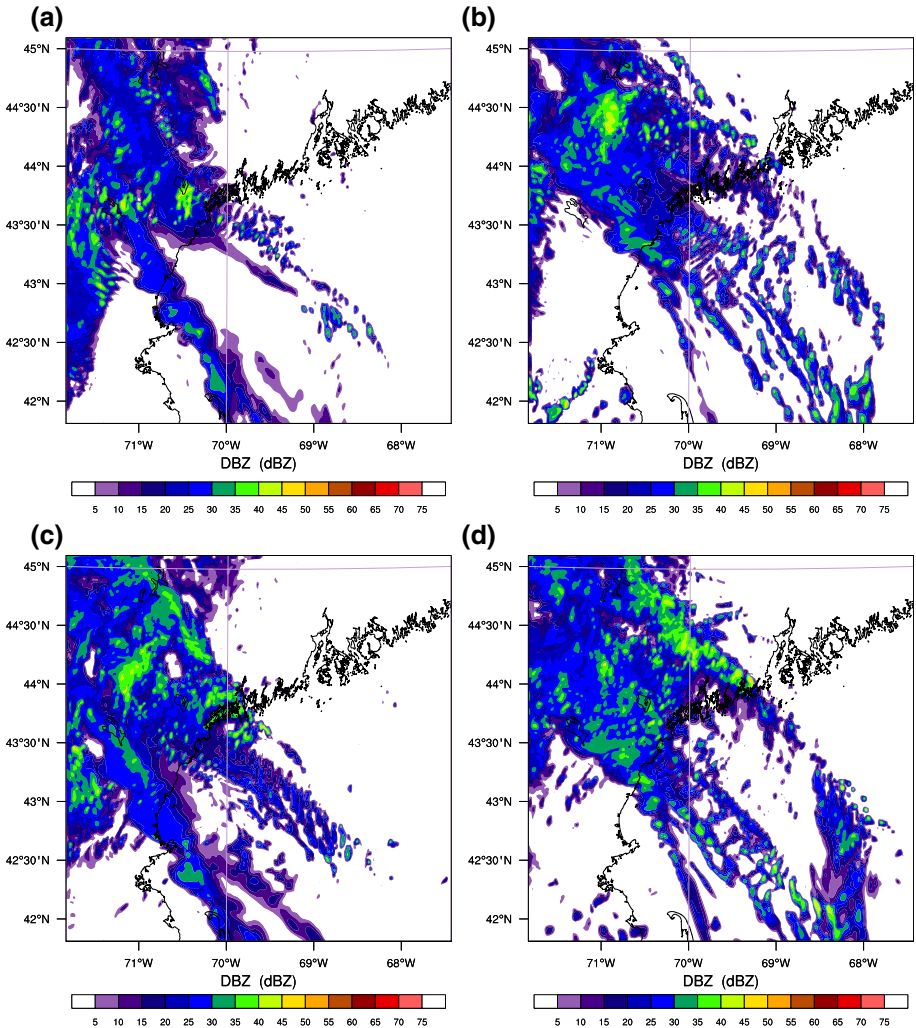


Fig. 7 Simulated radar reflectivity (DBZ) in WRF simulations at 18 UTC 28 October 2008 initiated at **a** 06 UTC 28 October 2008 and **c** 00 UTC 28 October 2008 and on 19 UTC 28 Oct 2008 initiated at **b** 06 UTC 28 October 2008 and **d** 00 UTC 28 October 2008. All simulations used ECMWF-OA initial and lateral boundary conditions

Table 3 List of experiments performed to assess the roles of different microphysics parameterizations

Exp. no.	13	14	15	16
Microphysics type	Morrison	Morrison	Lin (Purdue)	Lin (Purdue)
Nesting type	One-way	Two-way	One-way	Two-way

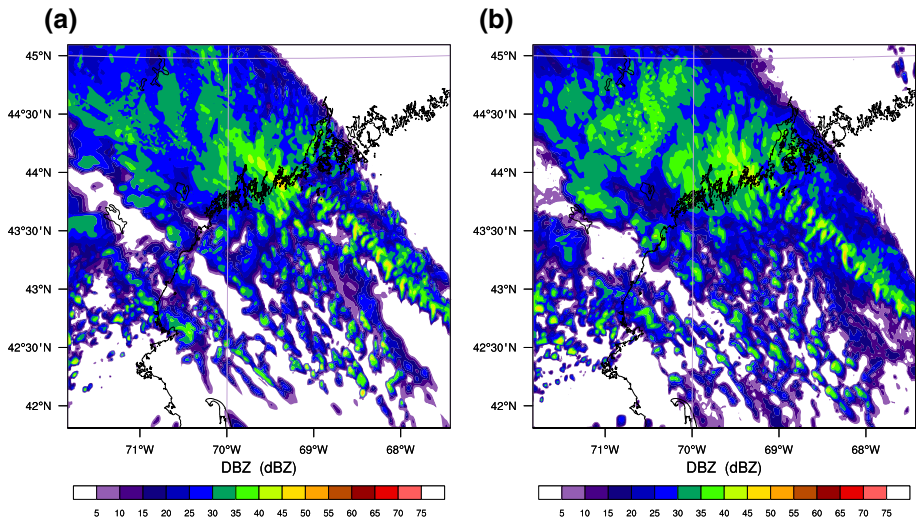


Fig. 8 Simulated radar reflectivity (DBZ) at 18:30 UTC 28 October 2008 for one-way nested WRF simulations using **a** Morrison and **b** Lin microphysics parameterizations

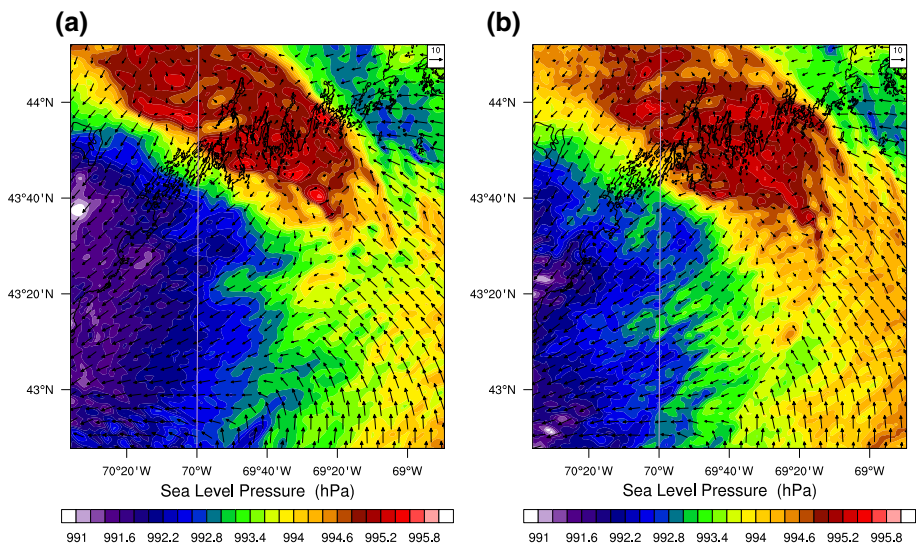


Fig. 9 Simulated MSLP (hPa) and 10-m wind vectors at 18:30 UTC 28 October 2008 for one-way nested WRF simulations using **a** Morrison and **b** Lin microphysics parameterizations

3.4 Sensitivity to convective parameterizations

Additional numerical experiments were performed to assess the sensitivity of the meso-scale simulations to the choice of the convective parameterization. Three different types of convective parameterizations were tested: Grell–Devenyi (GD) ensemble convective parameterization, which was used in the control simulation, Betts–Miller–Janjić (BMJ) and Kain–Fritsch (KF) convective parameterizations, all in one-way and two-way nesting setups (Table 4). The Morrison microphysics parameterization was used in all simulations. Convective parameterization was used only in the outermost domain ($dx = 9$ km) and was withheld in intermediate domain ($dx = 3$ km) and innermost domain ($dx = 1$ km).

Comparison of modelled and measured radar reflectivity suggests that the overall shape of reflectivity distribution around 18:30 UTC 28 October 2008 was well simulated in all numerical experiments (Fig. 10). In each of the simulations, main convection band was oriented southeast-northwest, and secondary convection area was located farther southwest of the precipitation band. However, a detailed look reveals some differences and inaccuracies. For example, the areas of high reflectivity were accurately represented in neither of the simulations. Furthermore, at 18:30 UTC 28 October 2008, all parameterizations produced too intense radar reflectivity offshore south of the observed precipitation system over the ocean (northeast of Provincetown). Only the numerical experiment with Kain–Fritsch parameterization simulated indices of wave-like radar reflectivity bands observed near the rear side of the precipitation band. Following subsequent evolution of the convective system, at 19 UTC, the distribution of convective activity was less accurate in simulations with BMJ parameterization than in other two simulations (not shown). In particular, while the radar images showed that the width of the observed convective zone was widened towards the southeast, simulated convective band in experiment with BMJ parameterization instead narrowed towards the southeast. Furthermore, the area without convective activity north of Provincetown was not represented well in either of the simulations. Thus, despite the above inaccuracies, rear side of the precipitation system was simulated over Boothbay around the time of meteotsunami as observed by radar imagery and numerical experiments with all three convective parameterizations simulated similar mesoscale structure of the precipitation zone.

Main mesoscale features of the mean sea-level pressure distributions at 18:30 UTC 28 October 2008 were similar all simulations (Fig. 11, compare with Fig. 9a). However, the details of the high-pressure band distribution that moved over Boothbay differed in both structure and intensity among sensitivity simulations. This was especially evident for surface pressure oscillations near the rear end of the precipitation system which was close to Boothbay at the time of meteotsunami. Namely, modelled surface pressure oscillations near the rear end of the high-pressure band were of small amplitudes in simulations with GD convective parameterization, while modelled surface pressure oscillations were of much higher amplitudes (up to 3 hPa) in simulations with KF convective parameterization.

In summary, gross features of simulated mesoscale precipitation system and MSLP were similar regardless of the choice of convective parameterization. However, the details in the precipitation system and the intensity of pressure oscillations within the high-pressure band did differ considerably, and WRF simulations using Kain–Fritsch convective parameterization appear to best represent the evolution of the precipitation system and the surface pressure oscillations. Thus, the choice of the convective parameterization may play an important role in simulating and predicting the details of atmospheric conditions during meteotsunami events.

Table 4 List of experiments performed to assess the roles of different convective parameterizations

Exp. no.	17	18	19	20	21	22
Convective parameterization	Grell–Devenyi	Grell–Devenyi	Betts–Miller–Janjić	Betts–Miller–Janjić	Kain–Fritch	Kain–Fritch
Nesting type	One-way	Two-way	One-way	Two-way	One-way	Two-way

3.5 Sensitivity to one-way and two-way nesting strategy

Throughout the above sensitivity simulations to address the roles of IC and LBC, simulation lead time, microphysics and convective parameterizations, one-way and two-way nested simulations were performed to assess the role of nesting strategy on the simulation results. For brevity, we here show results for two-way nested simulations using the ECMWF-OA as IC and LBC and initiated at 12 UTC 28 October 2008 and for choices of Grell–Devenyi and Morrison parameterizations (Fig. 12a), Grell–Devenyi and Lin parameterizations (Fig. 12b), Betts–Miller–Janjić and Morrison parameterizations (Fig. 12c) and Kain–Fritch and Morrison parameterizations (Fig. 12d).

Comparison of the results achieved with one-way and two-way nested simulations suggests a minor influence of the nesting strategy on the mesoscale flow evolution (cf. Figs. 9, 11). All simulations represented similar mesoscale evolution and structure of the surface pressure field regardless of the choice of nesting strategy. Nevertheless, subtle differences were found in the intensity of the mesoscale pressure system that moved over the area and in the structure of pressure oscillations within the precipitation zone. Concerning the localized nature of surface pressure oscillations related to meteotsunamis, it is apparent that the choice of nesting strategy may still play a role in simulating the exact details of the phenomenon.

4 Discussion and conclusions

Simulation of rapid short-wavelength pressure oscillations is challenging for mesoscale models and different simulations of this event showed a large scatter of results. According to performed verification with in situ, remote sensing and reanalysis data, WRF simulations using initial and lateral boundary conditions from ECMWF operational analysis seemed to perform better than simulations initiated with NARR and ERA-Interim reanalysis data. In fact, only these simulations reproduced well the precipitation zone that travelled from SSE to NNW and moved over the Boothbay Harbor area. Furthermore, the mesoscale setting and the precipitation system associated with the meteotsunami event were very sensitive to increasing the simulation lead time, suggesting the low predictability of mesoscale conditions favouring meteotsunamis. The choice of microphysics or convective parameterizations and the type of nesting strategy (one-way or two-way) was in this event not essential for simulating the mesoscale setting and evolution of the propagating precipitation band.

Numerical experiments with IC and LBC driven from ECMWF operational analysis which used the shortest simulation lead time were used to study the detailed numerical representation of surface pressure distribution near the Boothbay Harbor area. The representation of surface pressure oscillations near the rear end of the precipitation system was

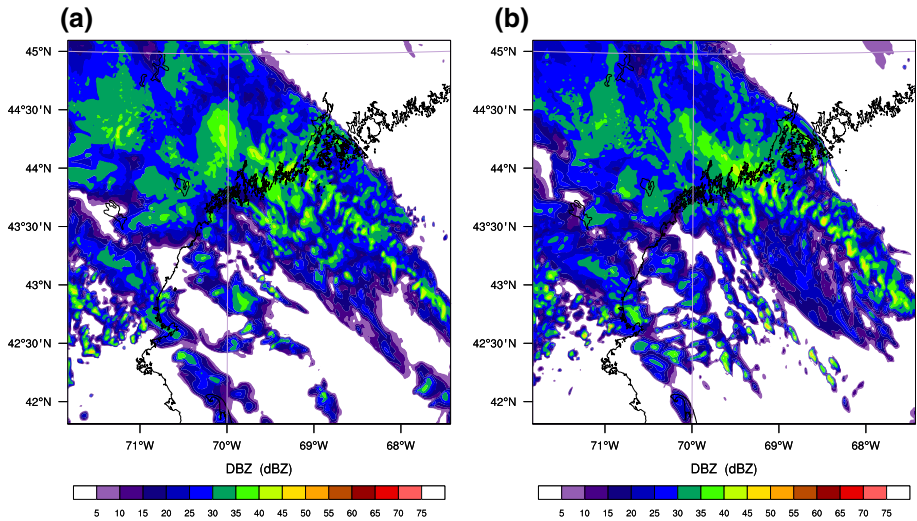


Fig. 10 Simulated radar reflectivity (DBZ) at 18:30 UTC 28 October 2008 for one-way nested WRF simulations using **a** Betts–Miller–Janjić and **b** Kain–Fritsch convective parameterizations. Compare with simulated radar reflectivity in simulation with Grell–Devenyi convective parameterization shown in Fig. 8a

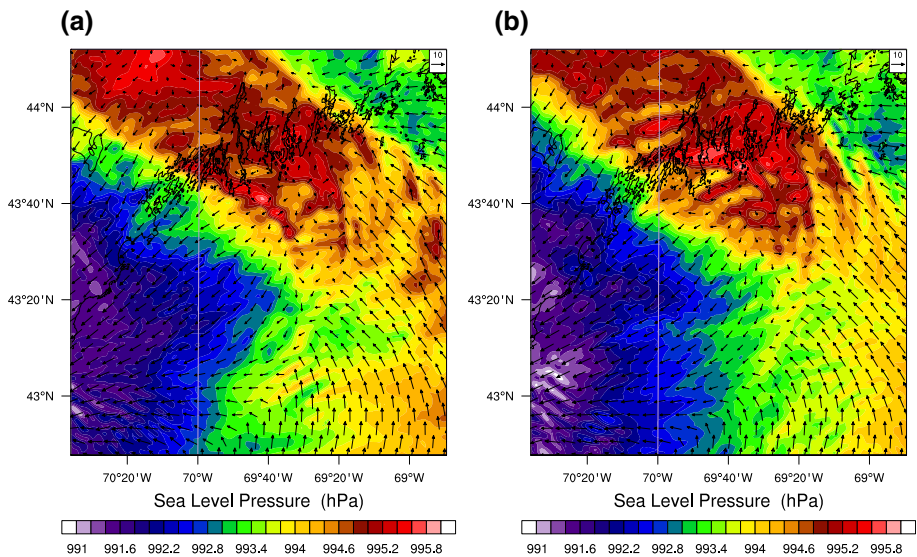


Fig. 11 Simulated MSLP (hPa) and 10-m wind vectors for one-way nested WRF simulations using **a** Betts–Miller–Janjić and **b** Kain–Fritsch convective parameterizations at 18:30 UTC 28 October 2008. Compare with simulated MSLP and 10-m wind vectors in simulation with Grell–Devenyi convective parameterization shown in Fig. 9a

very sensitive to the type of the convective parameterization chosen. On the other hand, the type of nesting feedback and microphysics parameterization showed lower sensitivity for representing the wave train of surface pressure oscillations. The latter may suggest that sedimentation and evaporation of rain, which are the key impacts of the two-moment

microphysics parameterizations (Morrison et al. 2009), were not crucial processes that determined the surface pressure oscillations in this event. Nevertheless, the choice of nesting strategy and microphysics parameterization may still modulate the exact properties of the surface pressure oscillation related to the studied meteotsunami.

Besides the effects of IC and LBC and simulation lead time on mesoscale setting, the most notable sensitivity was thus found for the choice of convective parameterization. Different convective parameterizations resulted in considerably different structure, organization and intensity of surface pressure oscillations. To some extent, this may be

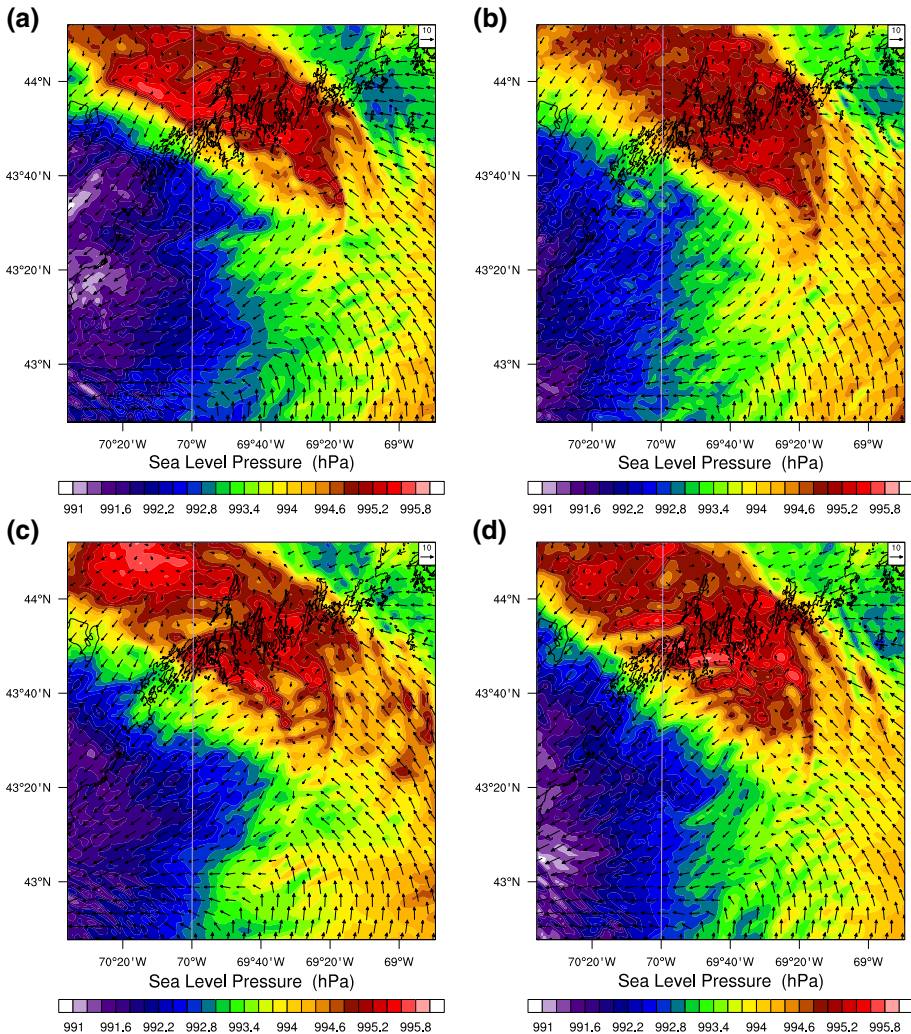


Fig. 12 Simulated MSLP (hPa) and 10-m wind vectors at 18:30 UTC 28 October 2008 for two-way nested WRF simulations using **a** Grell–Devenyi and Morrison parameterizations (compare with Fig. 9a), **b** Grell–Devenyi and Lin parameterizations (compare with Fig. 9b), **c** Betts–Miller–Janjić and Morrison parameterizations (compare with Fig. 11a) and **d** Kain–Fritsch and Morrison parameterizations (compare with Fig. 11b)

expected due to the fact that surface pressure oscillations and the related meteotsunami took place near the rear end of the precipitation system that propagated over Boothbay area. However, the analysis of surface pressure oscillations in this study predominantly utilized results from the innermost model domain, in which convective parameterization was withheld from the simulation. In both intermediate and innermost domains, heat and moisture tendencies and surface rainfall were determined by microphysics parameterization. Therefore, the effects of convective parameterization propagated from the outermost domain to the innermost domain during the simulation.

The large sensitivity of results to convective parameterizations likely results from their fundamentally different formulations. In the first place, these convective parameterizations use different types of closures, as outlined by Mapes (1997). Betts–Miller–Janjić is a representative of deep-layer control convective parameterizations which assume that the large-scale environment supplies convective available potential energy (CAPE) is efficiently consumed by convection. Kain–Fritsch parameterization is a representative of mass-flux low-level control convective parameterizations, since activation of convection is based on the low-level environment. Finally, Grell–Devenyi parameterization is a 144-member ensemble of mass-flux schemes consisting of large number of triggers and parameters, which is developed for somewhat coarser resolutions than the BMJ and KF schemes.

All types of convective parameterizations will generally tend to warm and dry the environment aloft, which may modulate synoptic and mesoscale conditions. Nevertheless, the differences among simulations with different schemes did exist. As mentioned in Sect. 3.4, numerical simulations with the BMJ scheme showed somewhat worse results than the other convective parameterizations. This may be related to the fact that even with moderate CAPE, the proper activation of the BMJ scheme depends on the deep moist layer (Gilland and Rowe 2012), which was not found in this event. Larger differences among convective parameterizations may also exist near the surface. For example, Kain–Fritsch parameterization will tend to cool the environment in the planetary boundary layer as opposed to Betts–Miller–Janjić parameterization (Stensrud 2007). These differences among convective parameterizations may influence the distribution of convective precipitation as well as the downward propagation of mid-tropospheric internal gravity waves and thus the related surface pressure oscillations. While the quantification of these effects during the Boothbay harbour event is out of scope of this paper, we note that convective parameterizations may have a profound effect on the low-level environment relevant for meteotsunamis.

In this numerical study, the best results are achieved in simulations where operational global analysis of atmospheric fields was used for initial and lateral boundary conditions. The operational analysis products are normally available in short (real) time and therefore may be used for eventual rapid assessment and forecast of meteotsunami favourable conditions in a meteotsunami warning system. Nevertheless, the ability of numerical weather prediction models to represent well internal gravity waves and convection depends also on the scale of the phenomena and grid spacing of the numerical weather prediction model. Besides numerical diffusion which increases the effective model resolution (Skamarock 2004), misrepresentation of internal gravity waves in certain conditions may be found even for grid spacing as small as 1/10 of the IGW wavelength (Schroeder and Schlünzen 2009). Therefore, weather prediction models used in meteotsunami warning systems should preferably operate on the order of 1-km grid spacing to explicitly represent the atmospheric conditions related to meteotsunamis, such as internal gravity waves and individual convective cells. Nonetheless, the usability of numerical weather prediction model at lower resolutions in meteotsunami warning systems should not be discarded as

these numerical predictions are extremely useful for identifying conditions for a duct or potentials for activation of convection.

In summary, the numerical weather prediction of atmospheric conditions related to meteotsunamis is attainable but challenging. It is encouraging that provided the accurate ICs and LBCs, the mesoscale models may, in addition to mesoscale conditions favourable for wave trapping, reproduce also the surface pressure oscillations jumps as well as wave trains of IGWs and related surface pressure oscillations. However, the success of mesoscale models according to this study appears limited to very short-range forecasting, most advanced parameterizations and very high-resolution grid spacing.

In addition, future meteotsunami warning systems should include several components in their architecture, from a network of microbarographs and high-density meteorological stations, through an assessment of synoptic conditions conducive for meteotsunami events, towards coupled numerical weather prediction mesoscale models and ocean models capable to reproduce the generated meteotsunami waves (Renault et al. 2011). The first system level may be based on assessment of the synoptic conditions, and once the favourable conditions are being detected, the modelling system may be executed in a burst mode, being run every 3 or 6 h to mitigate the influence of excessive forecast lead time. In parallel, the network of microbarographs and sea-level stations should be set also in burst mode, trying to detect eventual high-frequency air pressure or sea-level disturbance and assessing its characteristic towards the meteotsunami warning matrix (Šepić and Vilibić 2011). In addition, real-time detection of convective clouds and their movement may be initiated at certain frequency bands, as the convective clouds are found to be frequently connected to the meteotsunami events (Belušić and Strelec-Mahovic 2009). Such a multi-layer architecture of a meteotsunami warning system will presumably minimize false alarms and will allow for reliable and functional forecasting of potentially destructive meteotsunami events.

Acknowledgments We would like to thank NOAA and the Gulf of Maine Research Institute, in particular John Jensenius and Linda Mangum, who provided us with the data observed at GoMOOS/NERACOOS buoys during the event (<http://neracoos.org>). Croatian Meteorological and Hydrological Service accounted for the provision of computational resources for numerical simulations. This work was performed within the NOAA/NWS project “Towards a meteotsunami warning system along the US coastline (TMEWS)”, Award No. NA11NWS4670005. We are grateful to two anonymous reviewers for comments and suggestions that improved the manuscript.

References

- Belušić D, Strelec-Mahović N (2009) Detecting and following atmospheric disturbances with a potential to generate meteotsunamis in the Adriatic. *Phys Chem Earth* 34:918–927
- Belušić D, Grisogono B, Klaić ZB (2007) Atmospheric origin of the devastating coupled air–sea event in the east Adriatic. *J Geophys Res* 112:D17111. doi:[10.1029/2006JD008204](https://doi.org/10.1029/2006JD008204)
- Chen F, Dudhia J (2001) Coupling an advanced land surface-hydrology model with the Penn State-NCAR MM5 modeling system. Part I: model implementation and sensitivity. *Mon Weather Rev* 129:569–585
- Dudhia J (1989) Numerical study of convection observed during the winter monsoon experiment using a mesoscale two-dimensional model. *J Atmos Sci* 46:3077–3107
- Ek MB, Mitchell KE, Lin Y, Rogers E, Grunmann P, Koren V, Gayno G, Tarpley JD (2003) Implementation of Noah land surface model advances in the National Centers for Environmental Prediction operational mesoscale Eta model. *J Geophys Res* 108(D22):8851. doi:[10.1029/2002JD003296](https://doi.org/10.1029/2002JD003296)
- Gilland EK, Rowe CM (2012) A comparison of cumulus parameterization schemes in the WRF model. In: 2012 AMS annual meeting, P2.16. <https://ams.confex.com/ams/pdfpapers/120591.pdf>
- Hibiya T, Kajiura K (1982) Origin of the Abiki phenomenon (a kind of seiche) in Nagasaki Bay. *J Oceanogr Soc Jpn* 38:172–182

- Janjić ZI (2001) Nonsingular implementation of the Mellor–Yamada Level 2.5 scheme in the NCEP meso model. NCEP office note no. 437
- Jansà A, Monserrat S, Gomis D (2007) The rissaga of 15 June 2006 in Ciutadella (Menorca), a meteorological tsunami. *Adv Geosci* 12:1–4
- Laprise R (1992) The Euler equations of motion with hydrostatic-pressure as an independent variable. *Mon Weather Rev* 120:197–208
- Mapes BE (1997) Equilibrium vs. activation control of large-scale variations of tropical deep convection. In: Smith RK (ed) *The physics and parametrization of moist atmospheric convection*. Kluwer, Dordrecht, pp 321–358
- Mellor GL, Yamada T (1974) Hierarchy of turbulent closure models for planetary boundary-layers. *J Atmos Sci* 31:1791–1806
- Mellor GL, Yamada T (1982) Development of a turbulent closure-model for geophysical fluid problems. *Rev Geophys* 20:851–875
- Mlawer EJ, Taubman SJ, Brown PD, Iacono MJ, Clough SA (1997) Radiative transfer for inhomogeneous atmospheres: RRTM, a validated correlated-k model for the longwave. *J Geophys Res* 102:16663–16682. doi:[10.1029/97JD00237](https://doi.org/10.1029/97JD00237)
- Monserrat S, Ramis C, Thorpe AJ (1991) Large-amplitude pressure oscillations in the Western Mediterranean. *Geophys Res Lett* 18:183–186
- Monserrat S, Vilibić I, Rabinovich AB (2006) Meteotsunamis: atmospherically induced destructive ocean waves in the tsunami frequency band. *Nat Hazards Earth Syst Sci* 6:1035–1051
- Morrison H, Thompson G, Tatarskii V (2009) Impact of Cloud microphysics on the development of trailing stratiform precipitation in a simulated squall line: comparison of one- and two-moment schemes. *Mon Weather Rev* 137:991–1007
- Orlić M (1980) About a possible occurrence of the Proudman resonance in the Adriatic. *Thalassia Jugoslavica* 16(1):79–88
- Proudman J (1929) The effects on the sea of changes in atmospheric pressure. *Geophys Suppl Mon Notices R Astron Soc* 2(4):197–209
- Rabinovich AB (2009) Seiches and harbour oscillations. In: Kim YC (ed) *Handbook of coastal and ocean engineering*. World Scientific, Singapore, pp 193–236
- Renault L, Vizoso G, Jansà A, Wilkin J, Tintoré J (2011) Toward the predictability of meteotsunamis in the Balearic Sea using regional nested atmosphere and ocean models. *Geophys Res Lett* 38:L10601. doi:[10.1029/2011GL047361](https://doi.org/10.1029/2011GL047361)
- Schroeder G, Schlünzen KH (2009) Numerical dispersion of gravity waves. *Mon Weather Rev* 137:4344–4354
- Šepić J, Vilibić I (2011) The development and implementation of a real-time meteotsunami warning network for the Adriatic Sea. *Nat Hazards Earth Syst Sci* 11:83–91
- Šepić J, Vilibić I, Belušić D (2009) The source of the 2007 Ist meteotsunami (Adriatic Sea). *J Geophys Res* 114:C03016. doi:[10.1029/2008JC005092](https://doi.org/10.1029/2008JC005092)
- Šepić J, Vilibić I, Strelec Mahović N (2012) Northern Adriatic meteorological tsunamis: observations, link to the atmosphere, and predictability. *J Geophys Res* 117:C02002. doi:[10.1029/2011JC007608](https://doi.org/10.1029/2011JC007608)
- Skamarock WC (2004) Evaluating mesoscale NWP models using kinetic energy spectra. *Mon Weather Rev* 132:3019–3032
- Skamarock WC, Klemp JB (2008) A time-split nonhydrostatic atmospheric model for weather research and forecasting applications. *J Comput Phys* 227:3465–3485
- Stensrud DJ (2007) *Parametrization schemes: keys to understanding numerical weather prediction models*. Cambridge University Press, Cambridge
- Tanaka K (2010) Atmospheric pressure-wave bands around a cold front resulted in a meteotsunami in the East China Sea in February 2009. *Nat Hazards Earth Syst Sci* 10:2599–2610
- Vilibić I (2008) Numerical simulations of the Proudman resonance. *Cont Shelf Res* 28:574–581
- Vilibić I, Horvath K, Strelec Mahović N, Monserrat S, Marcos M, Amores A, Fine I (2014) Atmospheric processes responsible for generation of the 2008 Boothbay meteotsunami. *Nat Hazards*. doi:[10.1007/s11069-013-0811-y](https://doi.org/10.1007/s11069-013-0811-y). <http://link.springer.com/article/10.1007%2Fs11069-013-0811-y>